AD

AD 750081

REPORT NO. RG-TR-72-18

# SHOCK SHAPES IN GASEOUS SECONDARY INJECTION

by

A.R. Barbin and J.G. Williams

July 1972

*Approved for public release; distribution unlimited.*

U.S. ARMY MISSILE COMMAND

Redstone Arsenal, Alabama



DD FORM 1473, 1 DEC 68 PREVIOUS EDITION IS OBSOLETE

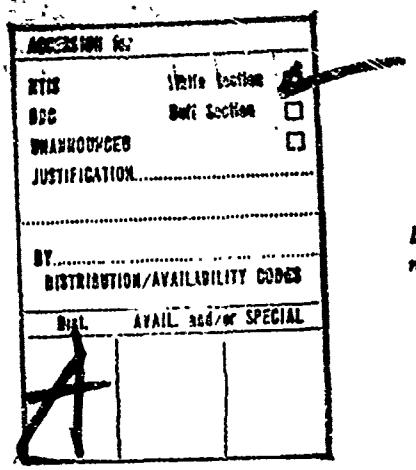


*DISPOSITION INSTRUCTIONS*

*Destroy this report when it is no longer needed. Do not return it to the originator.*

*DISCLAIMER*

*The findings in this report are not to be construed as an official Department of the Army position unless so designated by other authorized documents.*

*TRADE NAMES*

*Use of trade names or manufacturers in this report does not constitute an official indorsement or approval of the use of such commercial hardware or software.*

UNCLASSIFIED
Security Classification

## DOCUMENT CONTROL DATA - R & D

*(Security classification of title, body of abstract and indexing annotation must be entered when the overall report is classified)*

1. ORIGINATING ACTIVITY (Corporate author)
Guidance and Control Directorate
Directorate for Research, Development,
Engineering and Missile Systems Laboratory
U.S. Army Missile Command
Redstone Arsenal, Alabama 35809

2a. REPORT SECURITY CLASSIFICATION
Unclassified

2b. GROUP
N/A

3. REPORT TITLE
SHOCK SHAPES IN GASEOUS SECONDARY INJECTION

4. DESCRIPTIVE NOTES (Type of report and inclusive dates)
Technical Report

5. AUTHOR(S) (First name, middle initial, last name)
A. R. Barbin
J. G. Williams

| 6. REPORT DATE | 7a. TOTAL NO. OF PAGES | 7b. NO. OF REFS |
|---|---|---|
| 3 July 1972 | 42 | 14 |

| 8a. CONTRACT OR GRANT NO | 9a. ORIGINATOR'S REPORT NUMBER(S) |
|---|---|
| b. PROJECT NO. (DA) IT062114A645<br>AMC Management Structure Code No.<br>c 502P.11.71800<br>d | RG-TR-72-18<br>9b. OTHER REPORT NO(S) (Any other numbers that may be assigned this report)<br>AD |

10. DISTRIBUTION STATEMENT
Approved for public release; distribution unlimited.

| 11. SUPPLEMENTARY NOTES | 12. SPONSORING MILITARY ACTIVITY |
|---|---|
| None | Same as No. 1 |

13. ABSTRACT

The objective of this study was to develop a technique of predicting shock shapes and wall shock traces encountered in secondary injection into a conical rocket nozzle. The analysis is based on an analogy with Sakurai's second order blast wave theory, with allowance for axial variation in the free stream Mach number in the primary nozzle. Model tests indicate spreading of the shock adjacent to the wall slightly higher than expected. A procedure for shock prediction is presented based on one empirically determined constant. Independence of side forces in perpendicular secondary injection planes under conditions of shock intersection was experimentally verified.

DD FORM 1 NOV 68 1473 REPLACES DD FORM 1473, 1 JAN 64, WHICH IS OBSOLETE FOR ARMY USE.

UNCLASSIFIED
Security Classification

1-A

| 14 KEY WORDS | LINK A | | LINK B | | LINK C | |
|---|---|---|---|---|---|---|
| | ROLE | WT | ROLE | WT | ROLE | WT |
| Shock shapes<br>Gaseous secondary injection<br>Supersonic flow<br>Single port injection | | | | | | |

3 July 1972

Report No. RG-TR-72-18

# SHOCK SHAPES IN GASEOUS SECONDARY INJECTION

by

A.R. Barbin and J.G. Williams

DA Project No. 1T062114A645
AMC Management Structure Code No. 502P.11.71800

*Approved for public release; distribution unlimited.*

Guidance and Control Directorate
Directorate for Research, Development, Engineering
and Missile Systems Laboratory
Redstone Arsenal, Alabama 35809

IC

## ABSTRACT

The objective of this study was to develop a technique of predicting shock shapes and wall shock traces encountered in secondary injection into a conical rocket nozzle. The analysis is based on an analogy with Sakurai's second order blast wave theory, with allowance for axial variation in the free stream Mach number in the primary nozzle. Model tests indicate spreading of the shock adjacent to the wall slightly higher than expected. A procedure for shock prediction is presented based on one empirically determined constant. Independence of side forces in perpendicular secondary injection planes under conditions of shock intersection was experimentally verified.

## CONTENTS

## SYMBOLS

| | |
|---|---|
| $a$ | Local radius of primary nozzle |
| $A$ | Frontal area of equivalent blunt body |
| $A_1, A_2, A_3, C_1$ | Constants |
| $c$ | Sonic velocity |
| $Cp$ | Pressure coefficient, $\frac{P - P_\infty}{\frac{1}{2} \rho_\infty U_\infty^2}$ |
| $C_p^*$ | Pressure coefficient at nose of equivalent blunt body |
| $\bar{C}_D$ | Drag coefficient of equivalent blunt body |
| $d_e$ | Exit diameter of primary nozzle |
| $d_p^*$ | Throat diameter of primary nozzle |
| $d_s^*$ | Equivalent throat diameter of injected flow |
| $D$ | Drag force on equivalent blunt body |
| $E$ | Energy release per unit area of blast surface |
| $f(Z)$ | Correction factor to Z accounting for variation of Mach number along the primary nozzle |
| $J_o$ | Constant in Sakurai's second order blast wave solution |
| $\ell_1$ | Primary nozzle radius at the location of the shock apex |
| $L$ | Distance from primary nozzle exit to center of injection port, measured along the nozzle wall in a diametral plane |
| $\dot{m}_i$ | Mass flow rate of injectant |
| $\dot{m}_p$ | Mass flow rate of primary flow |
| $M$ | Mach number |
| $M_o$ | Mach number of primary stream at shock apex |
| $P$ | Pressure |

| | |
|---|---|
| $P^*$ | Pressure at nose of the blunt body |
| $r$ | Radius of equivalent blunt body |
| $R$ | Blast wave radius |
| $R_s$ | Radius of blast wave inside the primary nozzle |
| $K_o$ | Term in Sakurai's second order blast wave solution $\left(\frac{E}{p_\infty}\right)^{\frac{1}{(\alpha+1)}}$ |
| $U$ | Velocity |
| $x$ | Distance measured in a diametral plane along the primary nozzle wall from the apex of the separation line |
| $x^*$ | Distance measured in a diametral plane along the primary nozzle wall from the apex of the shock line |
| $Z$ | Distance downstream of the shock apex along a line passing through the shock apex and parallel to the primary nozzle centerline |
| $\alpha$ | Integer in Sakurai's second order blast wave solution $\alpha$=0, 1,2 corresponding to plane, cylindrical, and spherical shocks, respectively |
| $\beta$ | Angle between the local tangent to the surface of the equivalent blunt body and the undisturbed primary flow |
| $\beta^*$ | Value of $\beta$ at the nose of the equivalent blunt body |
| $\xi$ | Axial distance measured along the nozzle centerline from the throat |
| $\Delta$ | Shock standoff distance upstream of the nose of the equivalent blunt body measured along the primary nozzle wall |
| $\gamma$ | Ratio of heat capacities |
| $\lambda_1$, $\lambda_2$ | Constants in Sakurai's second order blast wave solution |
| $\phi$ | Azimuthal angle to shock trace on wall referenced to a diametral plane passing through the center of the injection port. The angle is measured clockwise looking forward. |
| $\rho$ | Density |

Subscripts

| | |
|---|---|
| $( )_{\infty}$ | Refers to conditions outside of the blast wave |
| $( )_{\infty i}$ | Refers to conditions outside of the blast wave at the center of the injection port |

## 1. Introduction

The first theoretical treatment of secondary injection was made by Ferrari [1] in a study of the forces produced by a lateral jet issuing from a cylindrical body into a supersonic flow past the body. Ferrari used Newtonian theory to predict the trajectory of the jet, shock stand-off distances, and pressure distributions; shock shapes were not determined experimentally. Amick and Hays [2] were the first to postulate a secondary injection flow model on the basis of experimental results. In tests of secondary injection from flat plates and cylindrical afterbodies, Amick and Hays identified separation zones and interaction shocks by means of a simple flow visualization technique.

The first attempt to correlate secondary injection shocks with blast waves was made by Broadwell [3] who utilized first order blast wave theory to predict shock shapes. Broadwell's analysis provided a good framework for data correlation, but significantly underpredicted measured side forces. The concept of treating the secondary injection jet as an equivalent blunt body was first put forth by Zukoski and Spaid [4] in a study of flat plate secondary injection; Schlieren techniques were utilized to determine bow shock profiles but no correlation of wall shock intersections were made.

A significant contribution toward formulation of a flow model applicable to secondary injection in a rocket nozzle was made by Charwat and Allegre [5]; these experiments identified separation and shock lines as well as strong vortex regions. The results were correlated by Hsia [6] and Hsia et al. [7] on the basis of second order blast wave theory. Hsia found that the data could be correlated with a blast wave from a line charge parallel to the nozzle centerline, having its origin at the location of the apex of the bow shock. A simpler correlation of shock shapes (and separation zones) was proposed by Wilson and Comparin [8] on the basis of tests run for NASA by Vickers [9]. In the Vickers tests, shocks were located by means of interpolation from rather sparsely populated pressure tap data and are not believed to be very accurate.

## 2. Statement of the Problem

Secondary injection of a fluid into the supersonic flow in a rocket nozzle alters the pressure distribution on the nozzle wall considerably because of the formation of a strong shock. Proper emplacement of injectors can thus be utilized to create desirable side forces. The design of such a thrust vectoring system requires accurate prediction of shock shapes and wall pressure distributions as functions of injection location and strength. The present study is concerned with the first problem, accurate determination of shock shapes.

Two previous investigations of shock shapes in the secondary injection in a conical rocket nozzle exist; these are the experiments by Charwat and Allegre [5] and the Vickers tests [9]. The experiments of Charwat and

Allegre were made in 5-degree conical nozzles under a limited range of operating parameters; those of the Vickers tests were made in a 15-degree conical nozzle. The second order blast wave analysis of Hsia et al. [7] correlates the Charwat and Allegre data, but is at variance with the Vickers tests. The present study was made to resolve this discrepancy and to determine an appropriate approach to analysis of shock shapes in 15-degree conical nozzles.

## 3. Experimental Approach

### a. Single Port Injection Studies

The shock experiments of this study were performed as part of a larger set of fluidic secondary injection experiments in which injection was accomplished by switching a bistable supersonic valve into opposite injector ports. In the present study, one of the ports was blocked with a shim to eliminate the possibility of spillover and to insure injection through a single port.

Figure 1 schematically depicts the experimental setup used in this study. A high pressure nitrogen supply was connected to a pressure regulator through a hand valve. The flow was remotely regulated by means of a fluidic resistive-capacitive circuit which varied the flow slowly from 0 psia to a maximum of approximately 1600 psia. The supply flow feeds the stagnation chamber for the primary nozzle and secondary injection circuit. During the shock experiments, the solenoid valve directed the control flow into the supersonic secondary injection valve so as to direct its output into the unblocked injector port.

Two steel primary nozzles were used in this study; dimensions and designations of these nozzles are given in Figure 2. The nozzles were identical except for the location of their injection ports. The primary nozzles were bolted onto the cylindrical stagnation chamber and sealed with a large O-ring.

Twelve experiments were conducted on single-port secondary injection, six with each of the two nozzles described in Figure 2. Secondary-to-primary flow rate ratios were varied by varying the nozzle throat diameter of the secondary injection valves (SIVN) and the control orifice diameter. Test conditions are summarized in Table I. The secondary throat diameters $d_s^*$ shown in Table I are equivalent diameters which account for the control flow through the solenoid into the secondary injection flow. The runs listed in Table I do not include those experiments which yielded no usable shock data (runs 1, 2, 7, and 9).

The method used to plot the shock traces on the nozzle wall was that first used by Amick and Hays [2]. Before each run, the inside of the nozzle was coated with a tacky mixture of china clay particles in methyl

Table I. Test Conditions, Single Injection Port Studies

| Run | L (in.) | $d^*_s$ (in.) | $\frac{\dot{m}_i}{\dot{m}_p} = \left(\frac{d^*_s}{d^*_p}\right)^2$ |
|---|---|---|---|
| 3 | 0.651 | 0.0976 | 0.0450 |
| 4 | 0.651 | 0.1496 | 0.1058 |
| 5 | 0.651 | 0.1533 | 0.1111 |
| 6 | 0.651 | 0.1845 | 0.1609 |
| 8 | 0.859 | 0.0736 | 0.0256 |
| 10 | 0.859 | 0.0976 | 0.0450 |
| 11 | 0.859 | 0.1030 | 0.0501 |
| 12 | 0.859 | 0.1536 | 0.1115 |

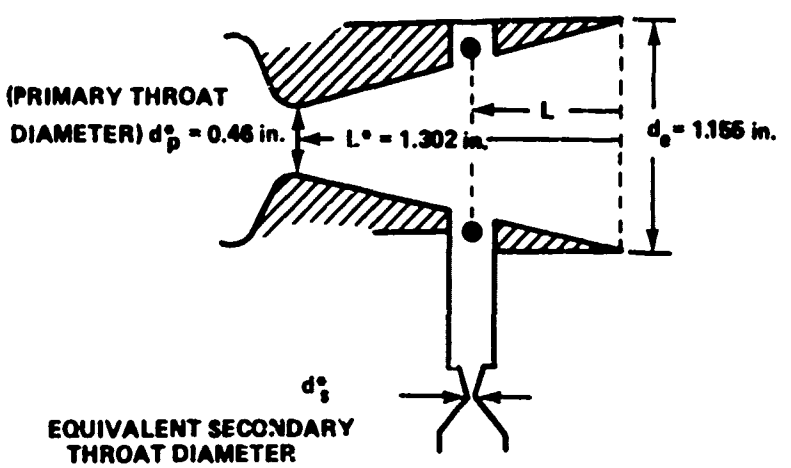


salicylate (Oil of Wintergreen) and a thin layer of dry china clay was blown on top of this mixture. Along the line where the shock intersected the wall, an area was scrubbed clean of the china clay during each run. Upon drying, this line showed up as a bare line on a background of white china clay. The trace was plotted by measuring the distance from the nozzle exit to the trace at 5-degree intervals of azimuthal angle. To facilitate the data taking, a special fixture was designed to fit onto the exit of the nozzle. This fixture had a rotating ring to measure and set the azimuthal angle to a probe which could be

moved along the wall; distances to the shock trace from the nozzle exit were measured with a machinist's scale mounted on the probe. The least count on the scale was 0.01 inch and the least count on the azimuth ring was 5 degrees.

b. Adjacent Port Injection Studies

Two additional experiments were run to determine the shock shapes existing in a nozzle with injection from two adjacent ports (90-degree azimuthal angle difference). The experimental setup was essentially the same as that described previously except that the injection ports were supplied directly by nozzles instead of supersonic bistable valves. Test conditions are listed in Table II. The shock trace data were collected as described previously.

Table II. Test Conditions, Adjacent Port Injection

| Run | L (in.) | $d^*_p$ (in.) | $d_e$ (in.) | $d^*_s$ (in.) | |
|---|---|---|---|---|---|
| | | | | Bottom Port | Left Port |
| 13 | 0.651 | 0.654 | 1.363 | 0.1442 | 0.1448 |
| 14 | 0.651 | 0.654 | 1.363 | 0.1442 | 0.089 |

## 4. Analysis of Shock Shapes

The formation of a shock in a supersonic stream caused by injection of a secondary fluid is analagous to the formation of a bow shock around an obstacle. The injected fluid must be turned downstream and accelerated through momentum interchange with the primary stream. Roughly, the penetration height of the secondary stream can be related to a dimension of some equivalent blunt body shape; the bow shock around this body may then be studied and related to the shock in the secondary injection. This approach has been used with some success by Hsia, et al. [6]. The development presented herein parallels, with slight modifications, the method used by Narasaki [10] in his study of the shocks around solid obstacles placed in a supersonic rocket nozzle.

Figure 3 depicts the shock shape in a diametral plane of a nozzle with secondary injection. The Z-axis is taken parallel to the nozzle centerline with its origin at the intersection point of the shock and the nozzle wall (upstream of the injection port). It is assumed that the shock shape is the result of a superposition of the primary nozzle flow and a shock wave emanating from a line charge along the Z-axis, the strength of which can be related to the size of the equivalent blunt body. Sakurai [11] derived the following relation between the radius R and the speed U of a shock front.

$$\left(\frac{c}{U}\right)^2\left(\frac{R_o}{R}\right)^{\alpha+1} = J_o\left[1 + \lambda_1\left(\frac{c}{U}\right)^2 + \frac{\lambda_2}{2}\left(\frac{c}{U}\right)^4 + \ldots\right] \qquad (1)$$

where $J_o$, $\lambda_1$, and $\lambda_2$ are constants and $\alpha = 0$, 1, and 2 correspond to plane, cylindrical, and spherical shocks, respectively. The sonic velocity of the undisturbed fluid outside the shock front is represented by c. The term $R_o$ in Equation (1) is given by

$$R_o = \left(\frac{E}{p_\infty}\right)^{\frac{1}{\alpha+1}} \qquad (2)$$

where E is the energy release per unit area of blast surface and $p_\infty$ is the pressure of the undisturbed fluid.

Equation (1) applies to a shock propagating into a quiescent fluid. As indicated in Figure 3, the primary flow in a nozzle sets up a standing shock with slope

$$\frac{dR_s}{dZ} = \frac{U}{U_\infty} = \frac{U}{cM} \qquad (3)$$

where $R_s$ is the radius of the standing shock and M is the Mach number of the primary (undisturbed) flow. Choosing $\alpha = 1$ (cylindrical shock front) and using only the second order term in (c/U), Equation (1) may be written as

$$\frac{1}{M^2}\left(\frac{dZ}{dR_s}\right)^2\left(\frac{R_o}{R_s}\right)^2 = J_o\left[1 + \frac{\lambda_1}{M^2}\left(\frac{dZ}{dR_s}\right)^2\right] \quad .$$

Rearranging and separating variables,

$$\left(R_o^2 - \lambda_1 J_o R_s^2\right)^{-\frac{1}{2}} R_s dR_s = \frac{1}{\sqrt{J_o}}\frac{dZ}{M} \qquad (4)$$

Equation (4) may be integrated from the shock apex (Z = 0) where $R_s = 0$ to a location Z downstream of the shock apex to yield

$$-\frac{R_o}{\gamma_1 J_o}\left[\sqrt{1-\gamma_1 J_o\left(\frac{R_s}{R_o}\right)^2}-1\right]=\frac{1}{\sqrt{J_o}}\int_{\xi_o}^{\xi_o+Z}\frac{d\xi}{M(\xi)} \tag{5}$$

where $\xi$ denotes centerline distance measured downstream from the nozzle throat and $\xi_o$ corresponds to the location of the shock apex. Defining f(Z) by the relation

$$f(Z)=\frac{M_o}{Z}\int_{\xi_o}^{\xi_o+Z}\frac{d\xi}{M(\xi)} \tag{6}$$

where $M_o$ denotes the free stream Mach number at the shock apex, Equation (5) can solved for $R_s$; thus,

$$\frac{R_s}{R_o}=\sqrt{\frac{2Zf(Z)}{M_o R_o\sqrt{J_o}}-\frac{\gamma-1}{M_o^2R_o^2}[Zf(Z)]^2}\quad . \tag{7}$$

Following Narasaki [10], the energy release per unit length per unit time, E is taken to be exactly twice the drag on the equivalent blunt body. Thus, $E = D/\pi$ and Equation (2) becomes

$$R_o=\sqrt{\frac{E}{p_\infty}}=\sqrt{\frac{D}{\pi p_\infty}} \tag{8}$$

where D is the drag on the equivalent blunt body of frontal area A,

$$D=\frac{\bar{C}_D A\rho_\infty U_\infty^2}{2}\quad . \tag{9}$$

In Equation (9), $\overline{C}_D$ represents a drag coefficient and the subscript $(\ )_\infty$ refers to conditions just ahead of the shock. Assuming the equivalent body to be a quarter sphere with a half-cylindrical afterbody, Equation (9) may be combined with Equation (7) to yield, with some manipulation,

$$\frac{R_s}{r} = C_1 \left( \frac{\overline{C}_D \gamma}{J_o} \right)^{\frac{1}{4}} \left\{ \frac{Zf(Z)}{r} - \frac{\gamma - 1}{M_o^2} \left( \frac{J_o}{\overline{C}_D \gamma} \right)^{\frac{1}{2}} \left[ \frac{Zf(Z)}{r} \right]^2 \right\}^{\frac{1}{2}} , \qquad (10)$$

where r represents the radius of the quarter sphere. Equation (10) differs from a similar equation quoted by Hsia et al [7] by the factor f(Z) which accounts for the variation of Mach number with Z and by the constant $C_1$ which has been added here as a constant to be determined from experiments.

The drag coefficient may be estimated by considering the pressure distribution on the nose of the equivalent blunt body (c.f., Figure 4). As suggested by Zukoski and Spaid [4] one may utilize Newtonian flow calculations, as modified by Lees [12], to get an expression for the pressure coefficient on the surface of the body

$$C_p = C_p^* \frac{\sin^2 \beta}{\sin^2 \beta^*} , \qquad (11)$$

where $\beta$ is the angle between the local tangent to the surface and the undisturbed primary flow and $C_p$ is defined by the relation

$$C_p = \frac{p - p_\infty}{\frac{1}{2} \rho_\infty U_\infty^2} , \qquad (12)$$

where the subscript $(\ )_\infty$ refers to conditions upstream of the bow shock. $C_p^*$ denotes the pressure coefficient at the point $\beta = \beta^*$. At the nose of the body $\beta^* = \pi/2$, and Equation (11) may thus be written

$$C_p = C_p^* \sin^2 \beta . \qquad (13)$$

The drag force can be found by integration of the pressure coefficient over the surface of the quarter sphere. Thus,

$$D = \bar{C}_D \, A \, \frac{1}{2} \rho_\infty U_\infty^2 = \iint_{A_s} \left( p - p_\infty \right) \cos \phi_s \, dA_s \tag{14}$$

where $\phi_s$ denotes the angle between the normal to the area element and the direction of the free stream; A is the projected area of the quarter sphere, $\pi r^2/2$. If an area element $dA_s$ is chosen as indicated in Figure 5,

$$dA_s = \pi r^2 \cos \beta \, d\beta$$

and

$$\cos \phi_s = \sin \beta \quad .$$

Thus, Equation (14) may be integrated

$$D = \frac{\bar{C}_D \, \pi r^2 \, \rho_\infty U_\infty^2}{4} = \int_0^{\pi/4} \frac{1}{2} Cp \, \rho_\infty U_\infty^2 \sin^3 \beta \cos \beta \, d\beta$$

or

$$\bar{C}_D = \frac{C_p^*}{2} \quad . \tag{15}$$

The pressure coefficient at the nose of the body may be evaluated as

$$C_p^* = \frac{\dfrac{p^*}{p_\infty} - 1}{\dfrac{\frac{1}{2} \rho_\infty U_\infty^2}{p_\infty}} = \frac{\dfrac{p^*}{p_\infty} - 1}{\frac{\gamma}{2} M_o^2} \tag{16}$$

where p* is the stagnation pressure behind a normal shock, easily calculated or read from tabulated data [13].

The equivalent blunt body radius r is found from an analysis of the momentum interchange between primary and secondary fluid streams. Taking the case of secondary injection normal to the nozzle centerline, it is assumed that the drag force D is that force required to accelerate the injected fluid to the primary stream velocity as it turns downstream. Thus,

$$D = \frac{\bar{C}_D A \rho_{\infty} U_{\infty i}^2}{2} = \dot{m}_i U_{\infty} \tag{17}$$

where $\dot{m}_i$ is the injectant flowrate and the subscript $( )_{\infty i}$ refers to undisturbed flow conditions at the injection station location. Equation (17) may be manipulated to yield

$$r = \left(\frac{4}{\pi} \frac{A_{\infty i}}{\bar{C}_D}\right)^{\frac{1}{2}} \left(\frac{\dot{m}_i}{\dot{m}_p}\right)^{\frac{1}{2}} \tag{18}$$

Upon substitution of Equation (17) into Equation (10) the following relation for $R_s$ results

$$R_3 = C_1 \left(\frac{4\gamma A_{\infty i} \dot{m}_i}{\pi J_o \dot{m}_p}\right)^{\frac{1}{4}} \left\{ Zf(Z) - \frac{\lambda_1}{M_o^2} \left(\frac{\pi J_o \dot{m}_p}{4\gamma A_{\infty i} m_i}\right)^{\frac{1}{2}} [Zf(Z)]^2 \right\}^{\frac{1}{2}} \tag{19}$$

Equation (19) illustrates the curious fact that $R_s$ does not depend on the drag coefficient $\bar{C}_D$. Presumably, one could use any convenient value; this has been pointed out previously by Hsia [6]. However, selection of $\bar{C}_D$ does affect the location of the shock apex and thus its value does influence the shape of the shock trace on the wall. It can also be shown that Equation (19) is independent of the shape assumed for the equivalent blunt body.

The shock standoff distance, from the nose of the equivalent blunt body, is most easily found by means of the simple correlation suggested by Ambrosio and Wortman [14]

$$\Delta = 0.143 \, r \, e^{3.24/M_o^2}$$

Equation (20) is based on data taken on spheres in supersonic air flows and, in spite of its simplicity, it is relatively accurate. Inasmuch as r depends on $\overline{C}_D$, Equation (20) shows that $\Delta$ also depends on $\overline{C}_D$; thus, one must have a relatively accurate $\overline{C}_D$ for an accurate estimate of shock apex location.

When using Equation (16), one does not know, a priori, the proper value of $M_o$, the Mach number at the apex of the shock, the location of which depends on $\overline{C}_D$. Thus, proper calculation requires an iterative scheme.

To relate the shock shapes in a diametral plane to observed shock traces on the nozzle wall we assume symmetry of the shock about the Z-axis (c.f. Figure 6). As illustrated in Figure 7, the location of the intersection of the shock with the nozzle wall at each axial location is simply the intersection point of two circles; one with center on the nozzle centerline and radius equal to the nozzle radius at that location, the other centered on the Z-axis with radius equal to the shock radius at that location. Thus, at the intersection point, the law of cosines yields

$$\phi = \text{Arc cos} \left( \frac{a^2 + \ell_1^2 - R_s^2}{2a\ell_1} \right) \tag{21}$$

where a represents the nozzle radius, $\ell_1$ is the nozzle radius at the shock apex, and $\phi$ is the azimuthal angle to the intersection point measured relative to a diametral plane through the centerline of the injection port.

The preceding development completes the second order blast wave analysis of shock shapes in a nozzle with secondary injection. Under a given set of conditions, the following procedure could be utilized to apply the theory:

a) Using the primary flow Mach number at the centerline of the injection port, calculate the drag coefficient $\overline{C}_D$, Equation (16).

b) Calculate the equivalent blunt body radius r from Equation (18) and the shock apex location $\Delta$ from Equation (20).

c) Using the Mach number $M_o$ evaluated at the shock apex found in step b), iterate steps a) and b) to the desired degree of accuracy.

d) Apply Equation (19) to calculate $R_s$ as a function of Z.

e) Calculate the location of the trace of the shock on the nozzle wall from Equation (21).

Inputs to the procedure previously detailed include: primary and secondary flow rates, nozzle geometry, and the constants $\lambda_1$, $J_o$ from Sakurai's solution [11]. For $\gamma = 1.4$, $\alpha = 1$,

$$\lambda_1 = -1.989$$

$$J_o = 0.877 \quad . \tag{22}$$

In evaluating $R_s$ as a function of Z (step d of the preceding procedure), from Equation (19), it is necessary to evaluate the function f(Z). Equation (6) defines this function as an integral involving the free stream Mach number. The variation of free stream Mach number with distance is plotted in Figure 8 for each of the primary nozzles used in this study. It was found that, with the exception of a short region near the throat, a good approximation to the Mach number variation is given by an expression of the form

$$M = A_1 + A_2 \xi - \left(A_1 - 1\right) e^{-A_3 \xi} \quad . \tag{23}$$

The specific expressions used in this study are compared to the actual Mach number variations in Figure 8.

## 5. Results and Discussion

### a. Shock Shapes, Single Port Injection

Data on shock patterns were gathered (as described in Section 3) in a series of twelve experiments conducted on two 15-degree conical nozzles. Both nozzles had identical throat and exit diameters of 0.460 and 1.155 inches, respectively; they differed only in the location of their injection ports (see Figure 2 and Table I for description and dimensions). The experiments covered a range of secondary-to-primary flow rate ratios from 2.5 to 16 percent. Nitrogen was used as the working fluid in all experiments.

Figures 9 through 12 depict the shock shapes for single port injection into the first nozzle (designation: SIV003) which had its injection port approximately midway between the throat and exit. The data for the second nozzle (SIV004), with injection port approximately one-third the nozzle length downstream of the throat, is illustrated in Figures 13 through 16. In both cases, the data are presented in the order of increasing injected flow rate. All of the curves shown are plotted on grids representing the unwrapped nozzle walls.

Several features were common to all the tests. First, considerable data loss was experienced. Thus, e.g., in Run 3 (Figure 9) only a short section of the china clay streak pattern was observed on one side of the injection port; presumably, the remainder of the china clay particles were blown off before the completion of the run. Coating of the nozzle with the china clay-methyl salicylate mixture before each run remained somewhat of an art throughout the experiments and data loss was experienced to some extent in all runs. Most of the wall traces consisted of bare areas on white backgrounds of the coating of china clay particles. Where discernible, the downstream edge of the bare area was more distinct than the upstream edge. In one case, the upstream edge was too faint to be accurately located (Run 6, Figure 12); in another (Run 8, Figure 13) the rear edge of the trace could not be located, apparently because the china clay particles were blown away during the run. In those runs where both edges of the trace could be accurately located (e.g., Run 5, Figure 11) the upstream and downstream edges tend to merge as the shock wraps around the wall. If the upstream edge is interpreted as the separation zone ahead of the shock at the rear edge of the trace, the merging of the two is anticipated in agreement with the results of Charwat and Allegre [5].

Comparisons of measured shock traces with those predicted by second order blast wave theory (presented in Section 4) are given in Figures 9 through 16. In general, overall agreement is fair if the rear edge of the measured trace is taken to be the bow shock and the constant $C_1$ is taken as 1.33 ($\sim \sqrt[4]{\pi}$). At the lower flow rate ratios, application of the theory is complicated by the size of the injection port (0.287-inch diameter in each case). The Mach number of the secondary fluid at the injection port is unknown; if it were assumed to be unity, the injectant stream would never completely fill the injection port. The procedure adopted was to take the injectant Mach number as unity and to consider the injectant strea to be exiting from the rear of the injection port. The shock standoff distance was then calculated relative to the centerline of that stream. In Runs 3, 8, 10, and 11 this procedure resulted in calculated shock apexes inside the injection port. For those cases the shock apex was arbitrarily taken at the upstream edge of the injection port, resulting in good agreement between measured and predicted shock shapes for Runs 10 and 11; Run 3 was not accurately predicted with this technique and Run 8 yielded no rear edge with which to compare.

Since $C_1 > 1$ for quantitative agreement between theory and experiment, it can be concluded that, near the wall, the shock spreads more rapidly than theory predicts. It is believed that this behavior is peculiar to the present geometry and is not to be extrapolated to other geometries.

Shock apex location was accurately predicted for Runs 4 and 5 by using the Mach number of the free stream at the center of the injection port area, assuming sonic injection, and performing the iteration described in Section 4. However, at the higher flow rate ratios (Runs 6 and 12) the location of the shock apex is drastically over predicted by

theory and no rational method of accurately predicting shock apex location was found; the theoretical curves were forced to pass through the measured apexes in those cases.

Insufficient simultaneous data on separation and bow shocks exist to get a correlation between the two. Run 5 indicates, however, that the two are separated at the shock apex by approximately 1.5 r. The Wilson and Comparin [8] estimate of this distance is 1.75 r; their correlation of the separation line is

$$\left(\frac{a\phi}{r}\right) = 1.5\left(\frac{x}{r}\right)^{0.7} \tag{24}$$

where x denotes distance along the wall from the apex of the separation line. This relation predicts a separation line which diverges from the bow shock, whereas measurements indicate a merging of the two. No attempt was made to improve this correlation.

The modification of second order blast wave theory to account for a varying free stream Mach number results in a slight improvement as illustrated in Figure 11 for Run 5. As indicated, if no correction is made for variation of free stream Mach number (i.e., f = 1), the theory drastically overpredicts the shock spread. For the conditions of Run 5, in fact, shock impingement on the opposite nozzle wall is predicted but not measured.

Wilson and Comparin [8] proposed the following correlation of shock shapes:

$$\left(\frac{a\phi}{r}\right) = 1.12\left(\frac{x^*}{r}\right)^{0.535} \tag{25}$$

where $(a\phi)$ represents the distance measured along the wall from a diametral plane passing through the centerline of the injection port and $x^*$ is the distance along the wall, in that diametral plane, measured from the shock apex. As illustrated in Figure 11, Equation (25) drastically underpredicts the spread of the shock. It was found that at the lower flow rates (less than 10 percent of the primary flow) a fair correlation of shock shapes could be obtained if the constant 1.12 in Equation (25) is changed to 2.13. A number of these curves are shown in Figures 9 through 12.

b. Shock Shapes, Adjacent Port Injection

Two experiments were conducted with injection from two adjacent ports (90-degrees azimuthal angle separation). These experiments were run on a 15-degree conical nozzle with a 0.654-inch diameter throat and a 1.363-inch diameter exit (designated SIV006). The first-run

was made with nearly identical injection nozzles (designated SIVN002-1, SIVN001-2); the second run was made with injection nozzles of significantly different throat diameters (SIVN006, SIVN002-2). A complete listing of all geometry is shown in Table II.

The results of the first run, with nearly identical nozzles (i.e., a symmetrical shock pattern), is shown in Figure 17 together with the shock shapes predicted with second order blast wave theory. Agreement between the measurements and predictions is good. Downstream of the intersection point (at 45 degrees) is a slip line extending to the exit of the nozzle. Shock reflections would be anticipated for such an intersection, but these were not detected in the present series of measurements.

Measured and predicted shock shapes for the second run, with an asymmetrical pattern, are given in Figure 18. Again, the agreement is good. In this case the shock intersection occurs at 52 degrees left of the injector port, at the bottom of the nozzle, yet the slip line runs straight back to the exit. In both tests the slip line downstream of the intersection point was exceptionally clear.

In Figures 17 and 18, the predicted shock shapes based on second order blast wave theory, were forced to pass through the measured apexes of the shock traces. The shock apexes were again slightly overpredicted (0.09 inch).

An important bonus was derived from the shock intersection tests. Side force measurements were made with each port off, each port on, and both ports on. These measurements indicate zero coupling of side forces, even though the bow shocks intersected. These results agree with the force measurements of the Vickers tests [9].

All of the data previously presented were found to be reproducible to within 0.01 inch, the least count on the scale used to position the probe.

## 6. Conclusions

The results of this study lead to the following conclusions concerning shocks in secondary injection into 15-degree conical nozzles:

a) The shape of the shock trace on the nozzle wall is well represented by a second order blast wave analysis, which accounts for variation of free stream Mach number along the nozzle centerline except for those cases where the injection ports do not flow full. Good quantitative agreement between theory and experiment was obtained by proper choice of the empirical constant $C_1$ ($\approx \sqrt[4]{\pi}$ for the present geometry).

b) A separation shock exists a short distance upstream of the shock trace on the wall (within 1.5 r). This separation shock merges with the bow shock as it wraps around the wall of the nozzle.

c) The intersection point of the bow shocks in adjacent port injection can be accurately predicted by second order blast wave theory. Measurements indicate a slip line extending straight downstream from this point to the exit, even with unequal strength shocks.

d) The side force produced by secondary injection from one port is completely unaffected by injection from an adjacent (90 degrees) port with or without bow shock intersection.

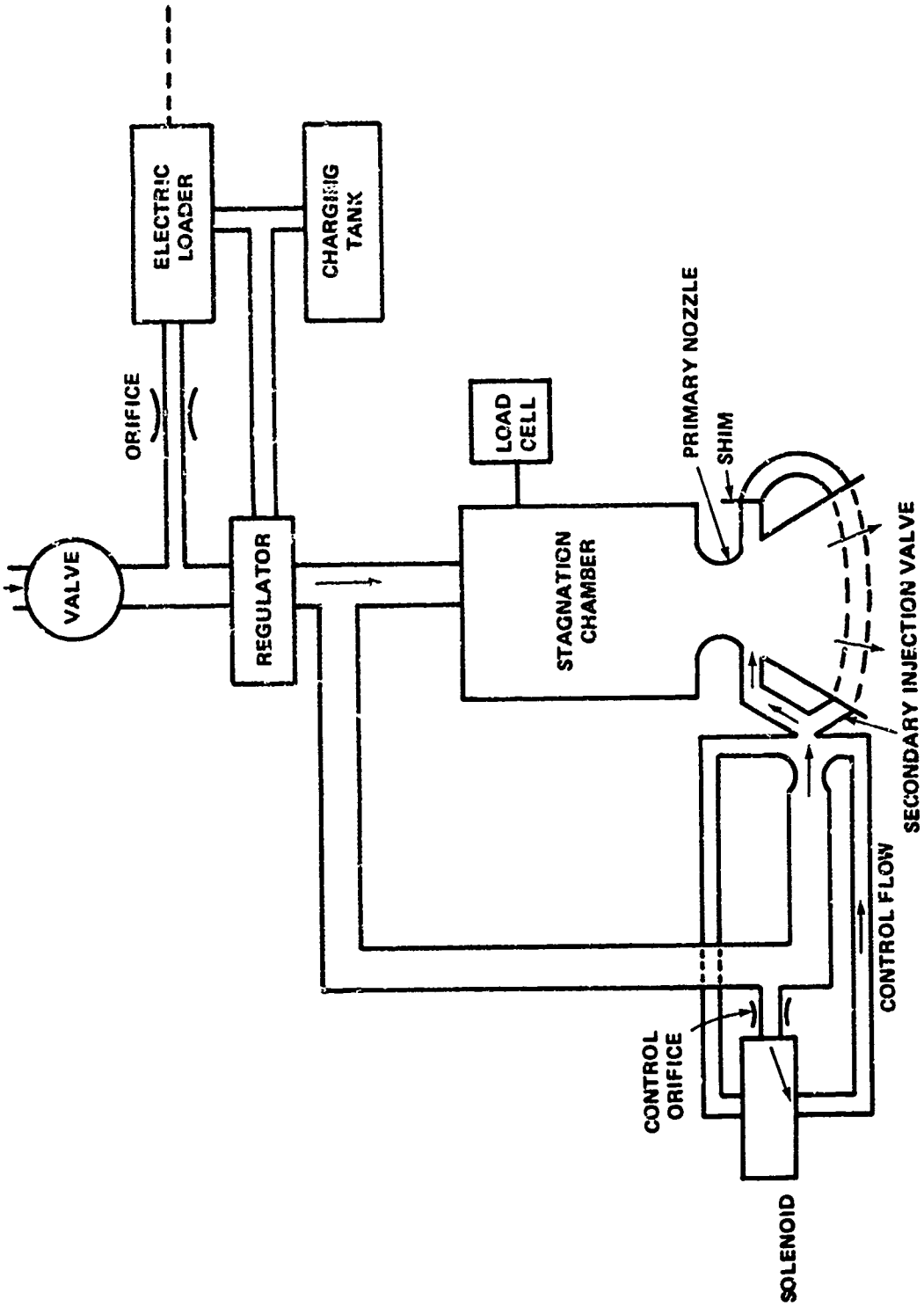


Figure 1. Experimental Setup

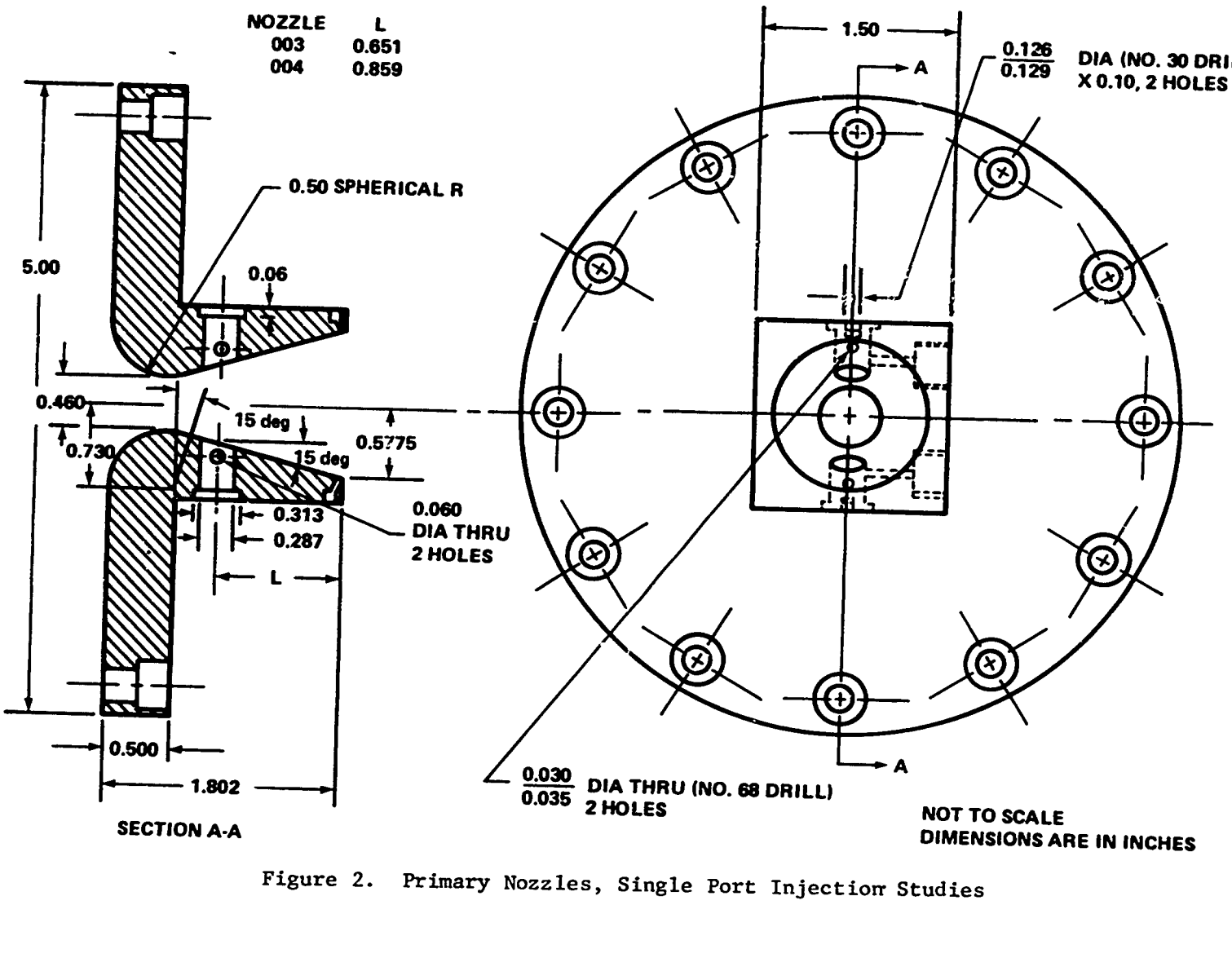


Figure 2. Primary Nozzles, Single Port Injection Studies

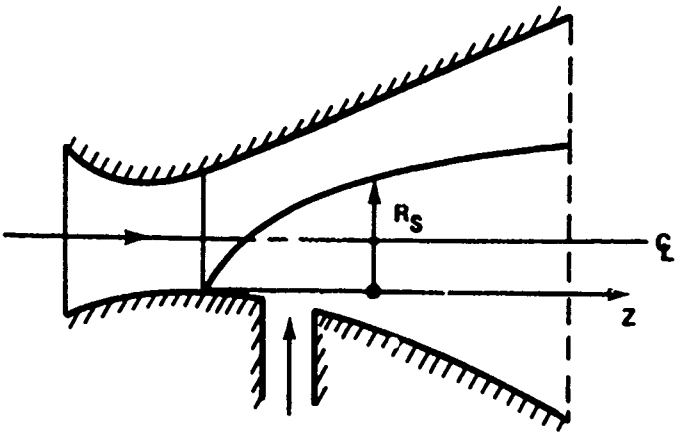


Figure 3. Shock Shape, Diametral Plane

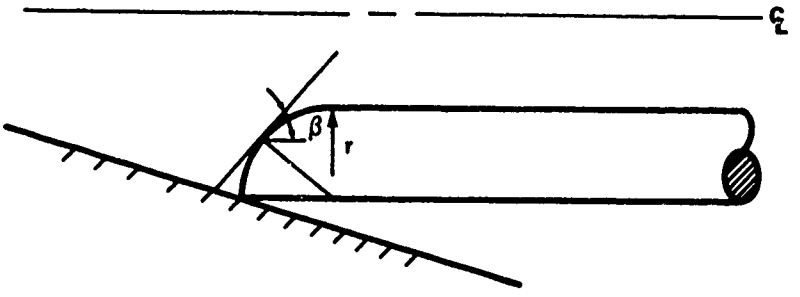


Figure 4. Equivalent Blunt Body

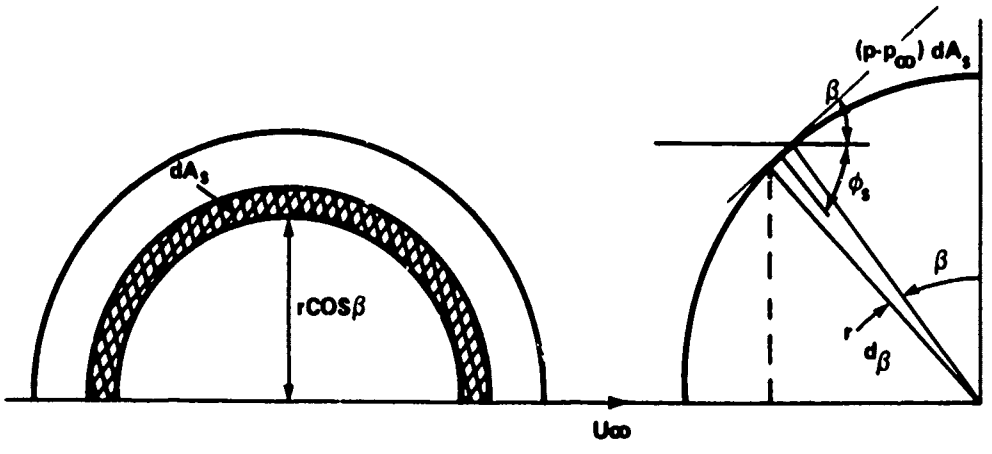


Figure 5. Calculation of Drag Force on Quarter-Sphere

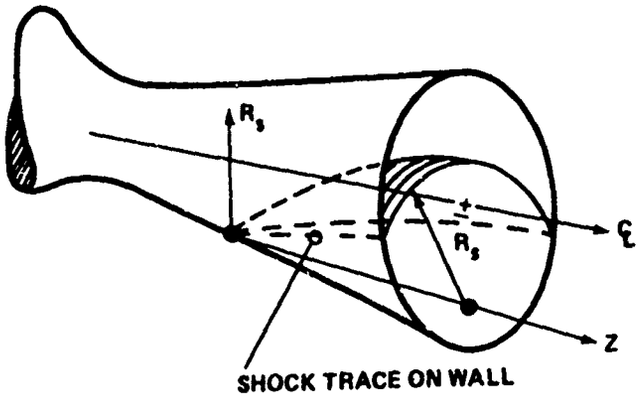


Figure 6. Shock Envelope in Nozzle

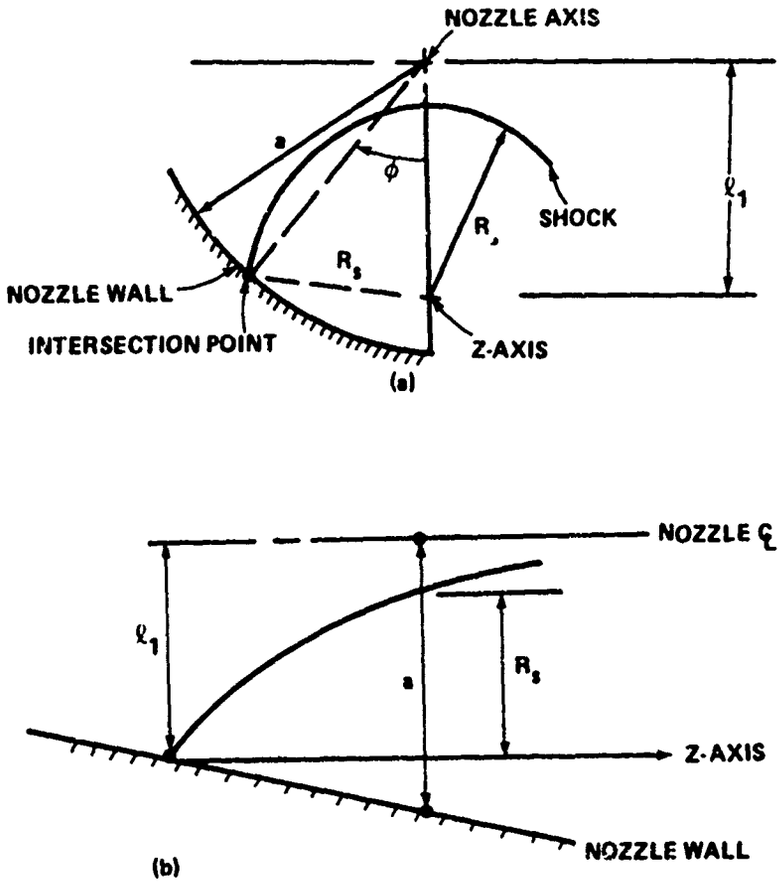


Figure 7. Location of Shock Trace on Nozzle Wall

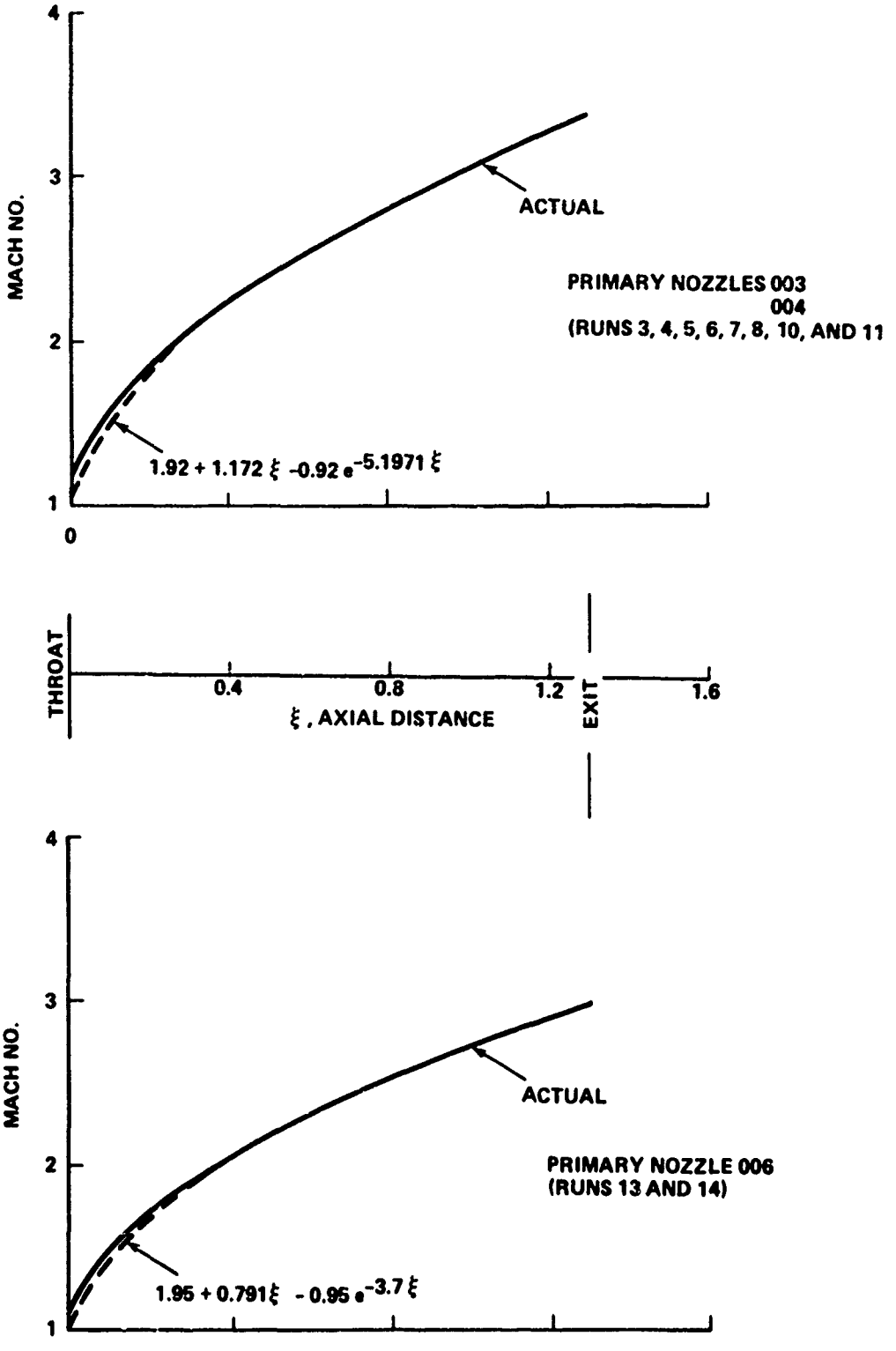


Figure 8. Mach Number Versus Axial Distance from Throat

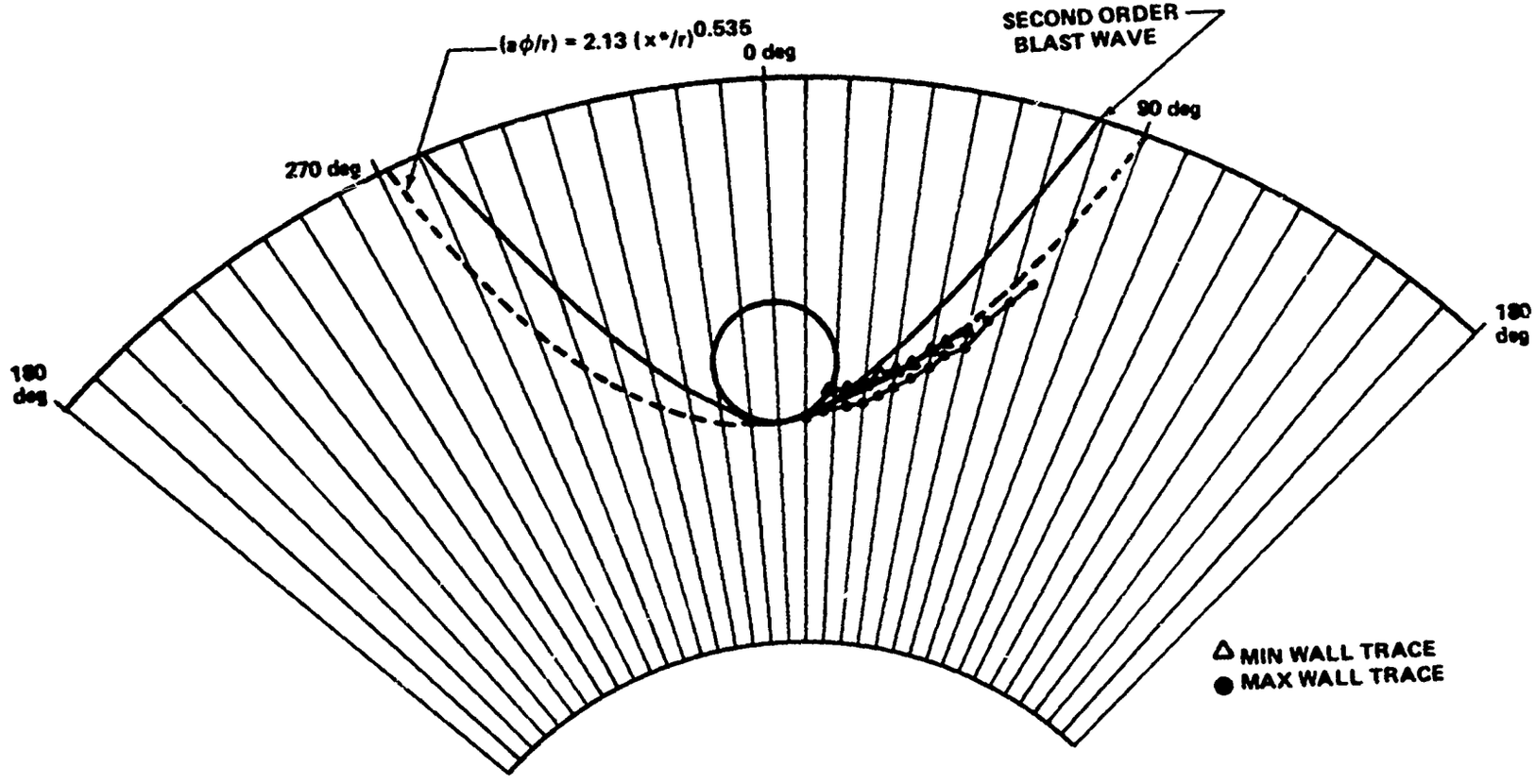


Figure 9. Shock Traces, Run 3

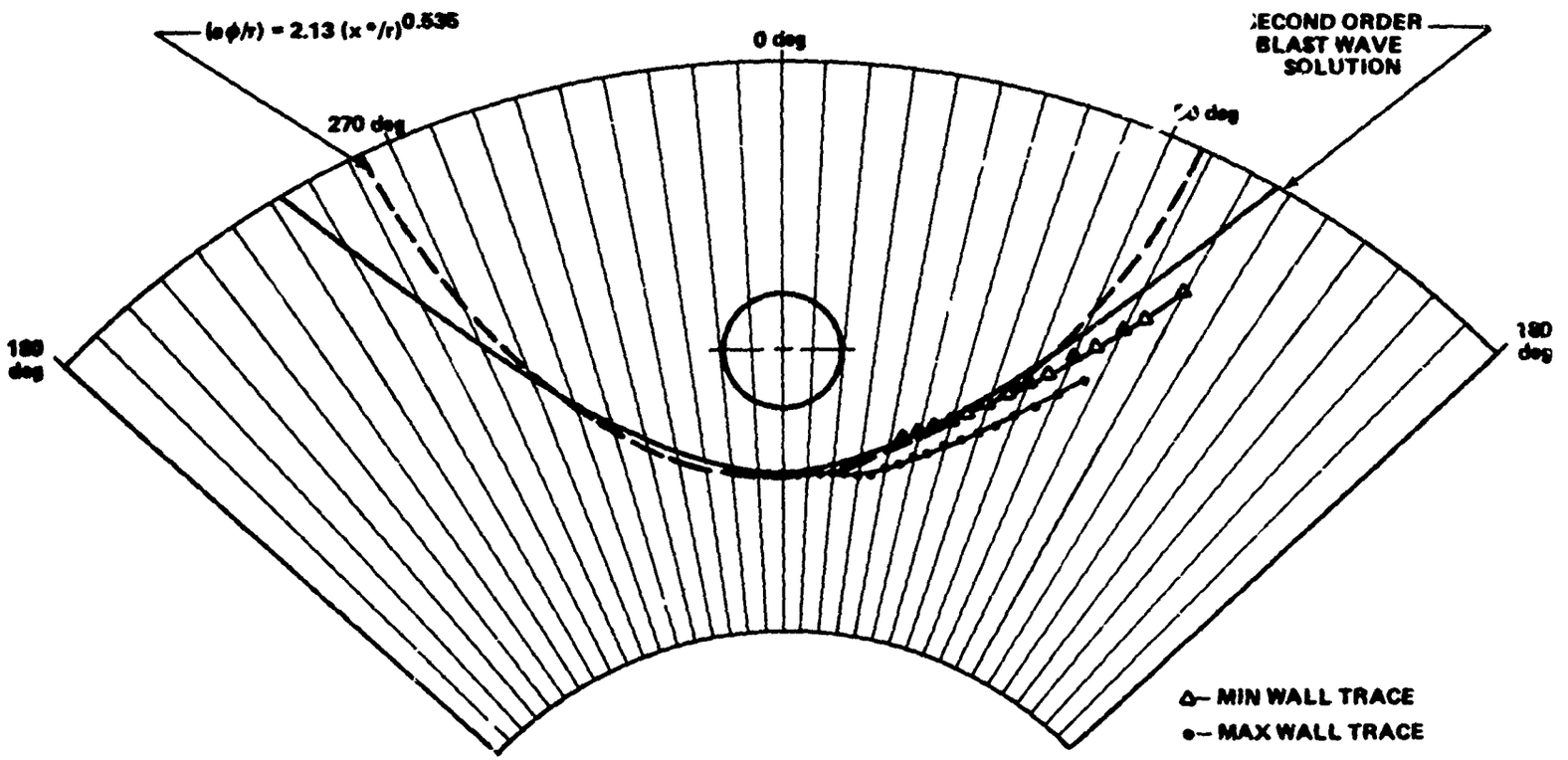


Figure 10. Shock Traces, Run 4

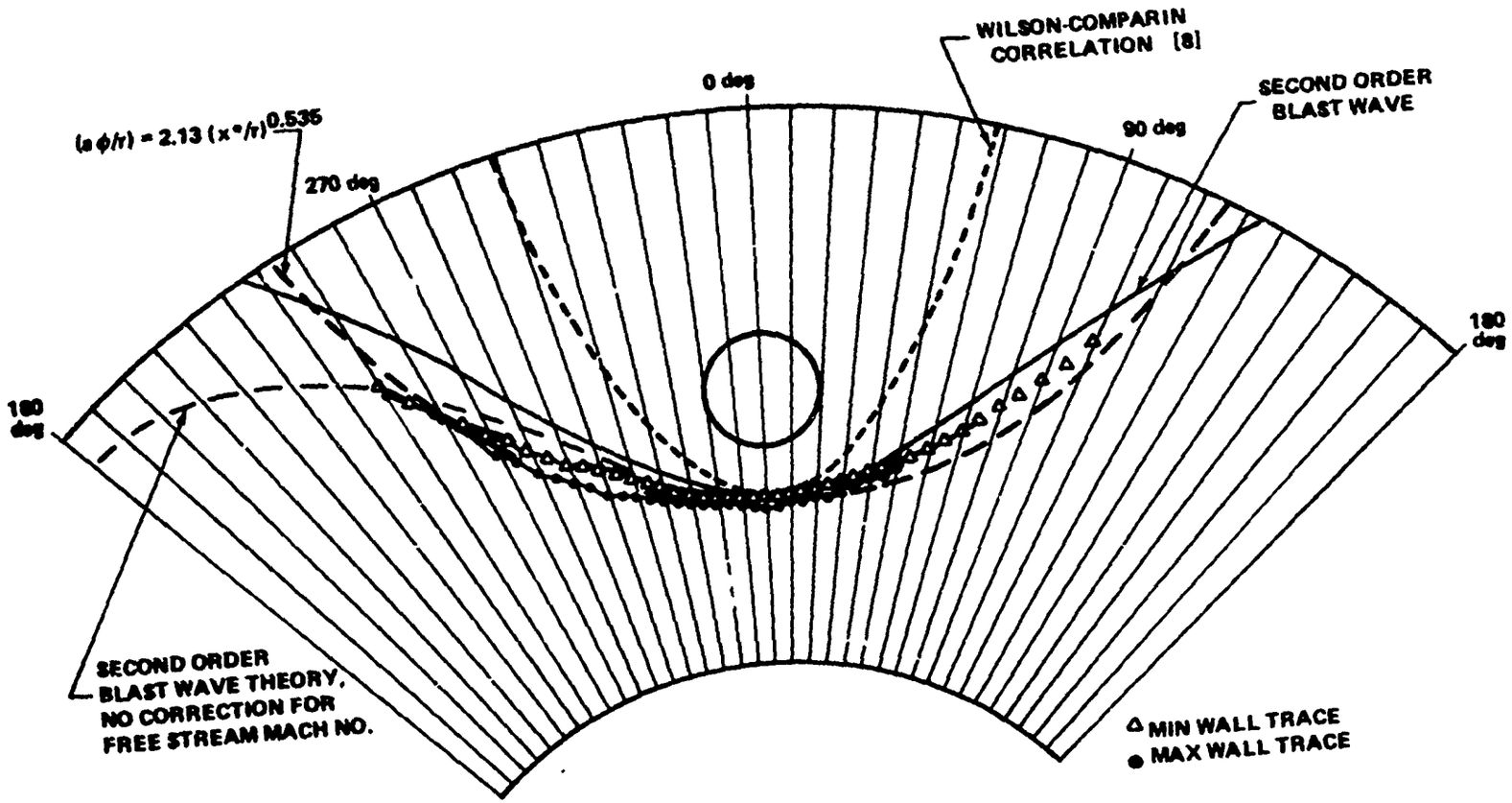


Figure 11. Shock Traces, Run 5

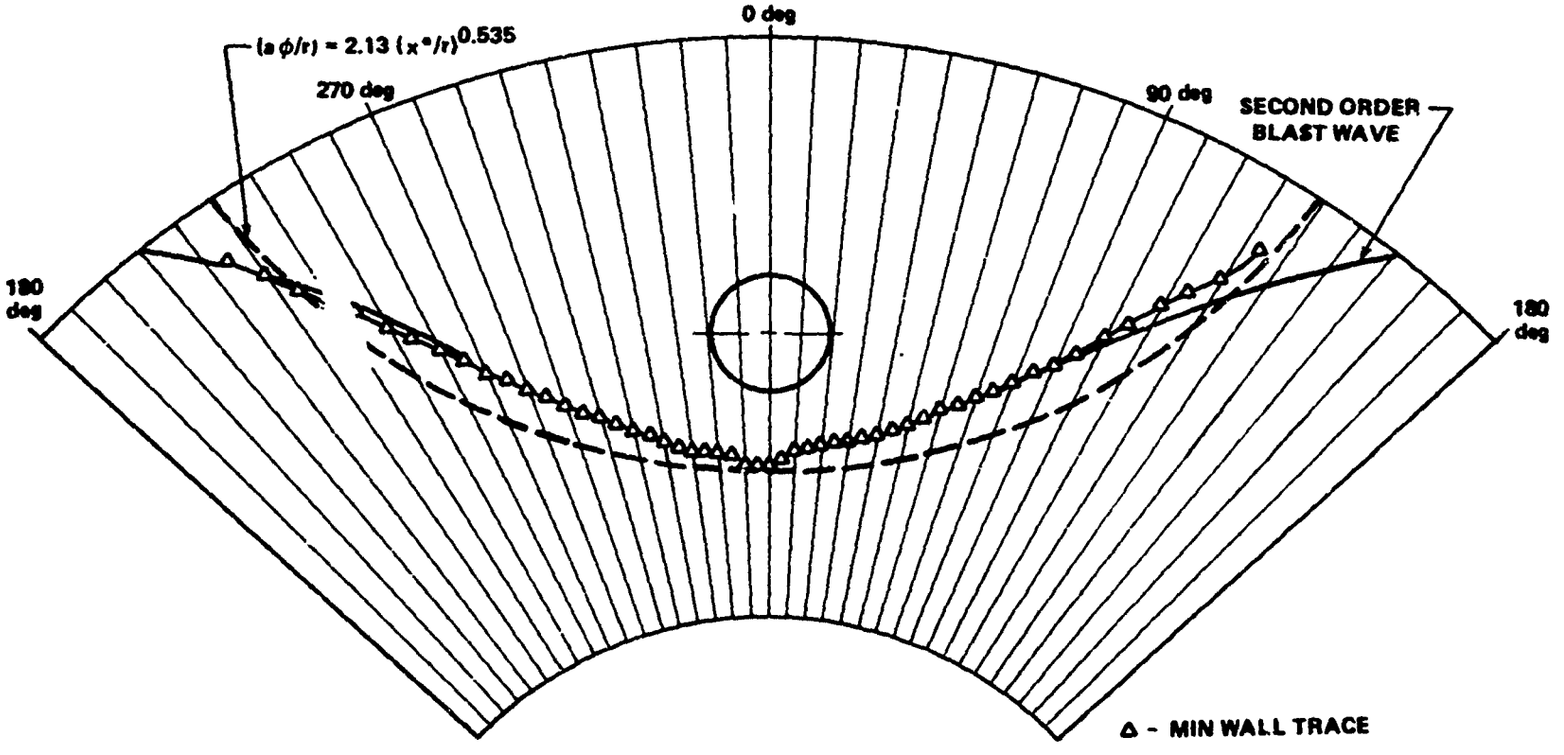


Figure 12. Shock Traces, Run 6

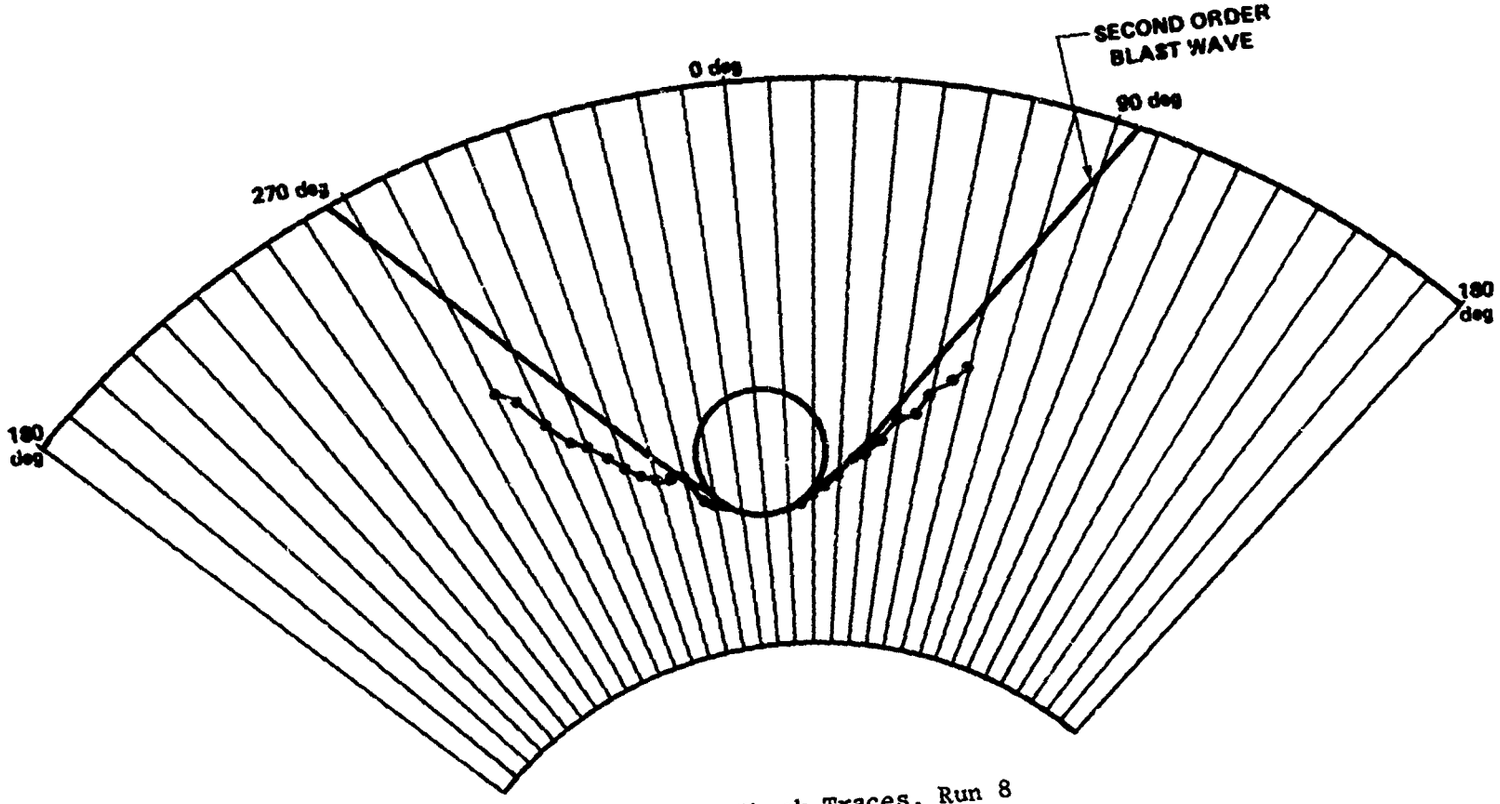


Figure 13. Shock Traces, Run 8

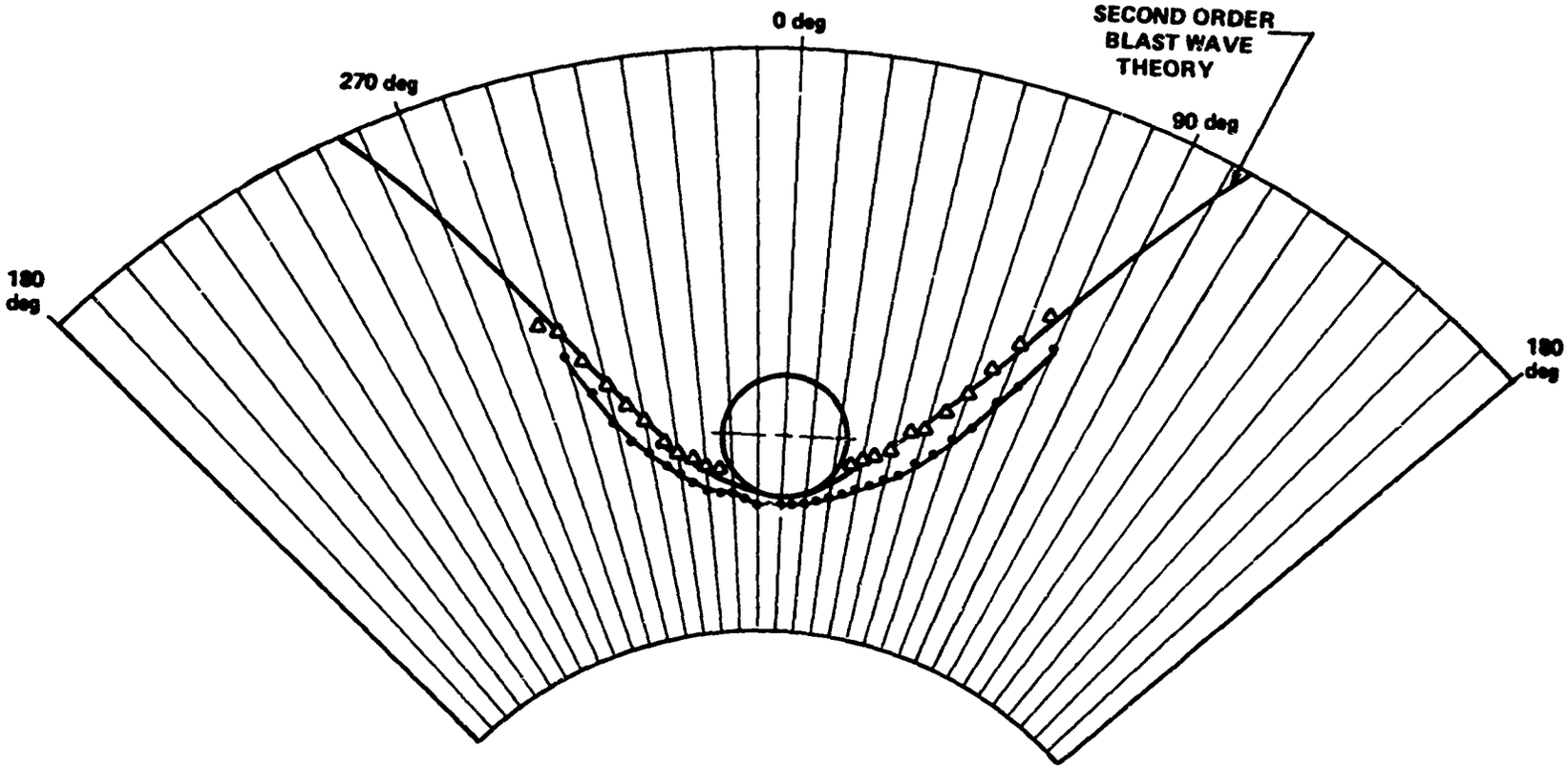


Figure 14. Shock Traces, Run 10

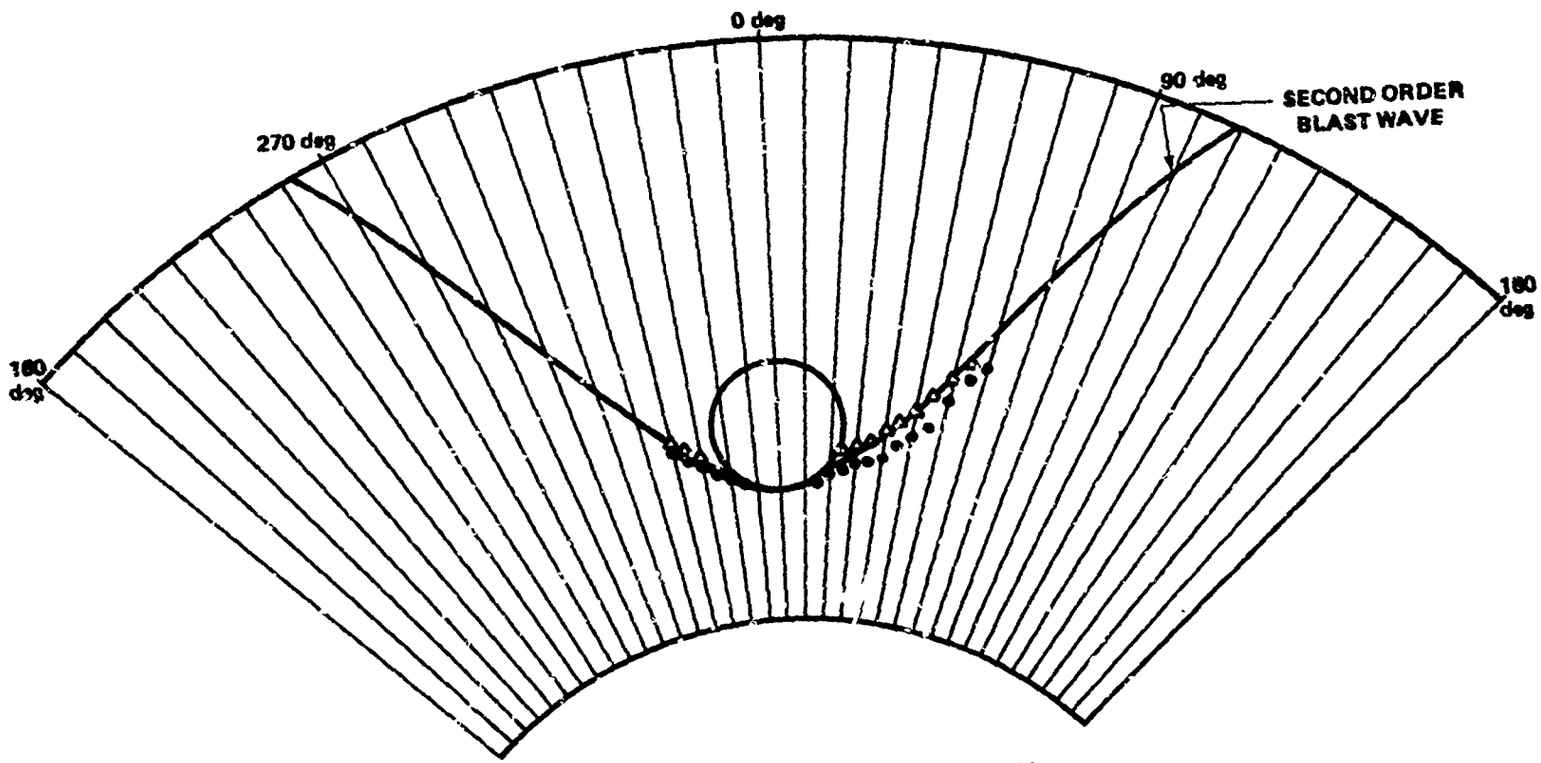


Figure 15. Shock Traces, Run 11

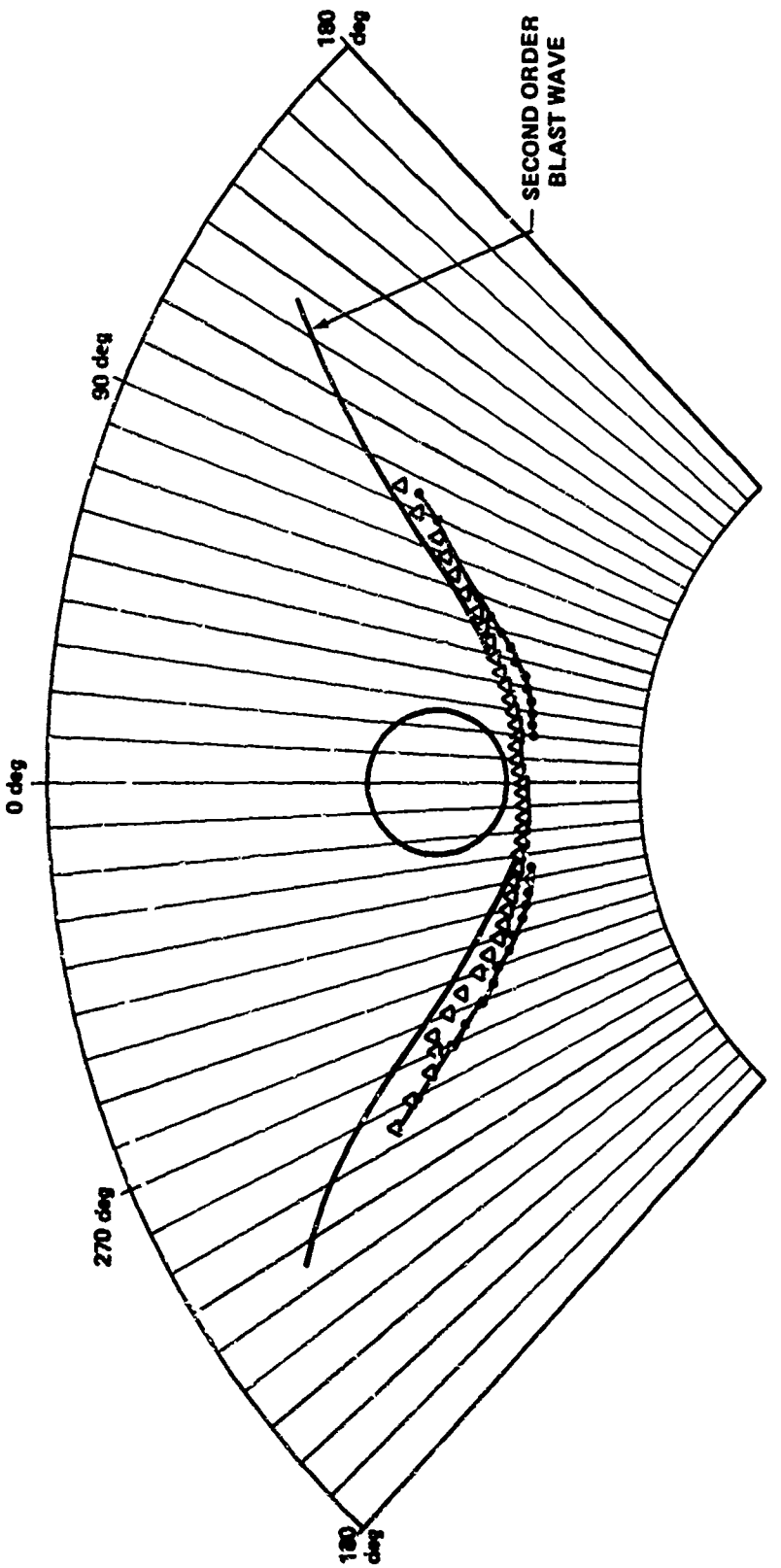


Figure 16. Shock Traces, Run 12

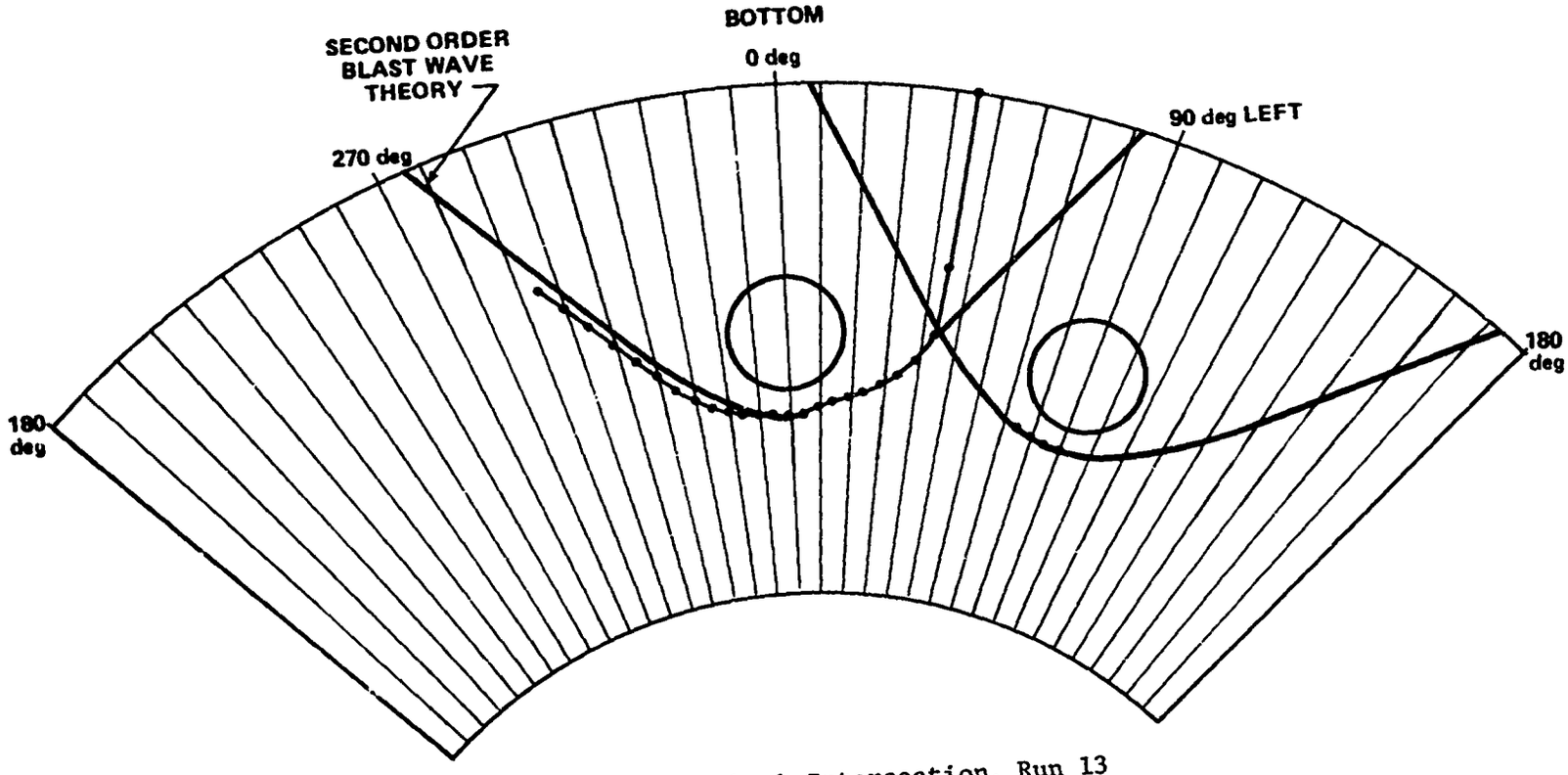


Figure 17. Shock Intersection, Run 13

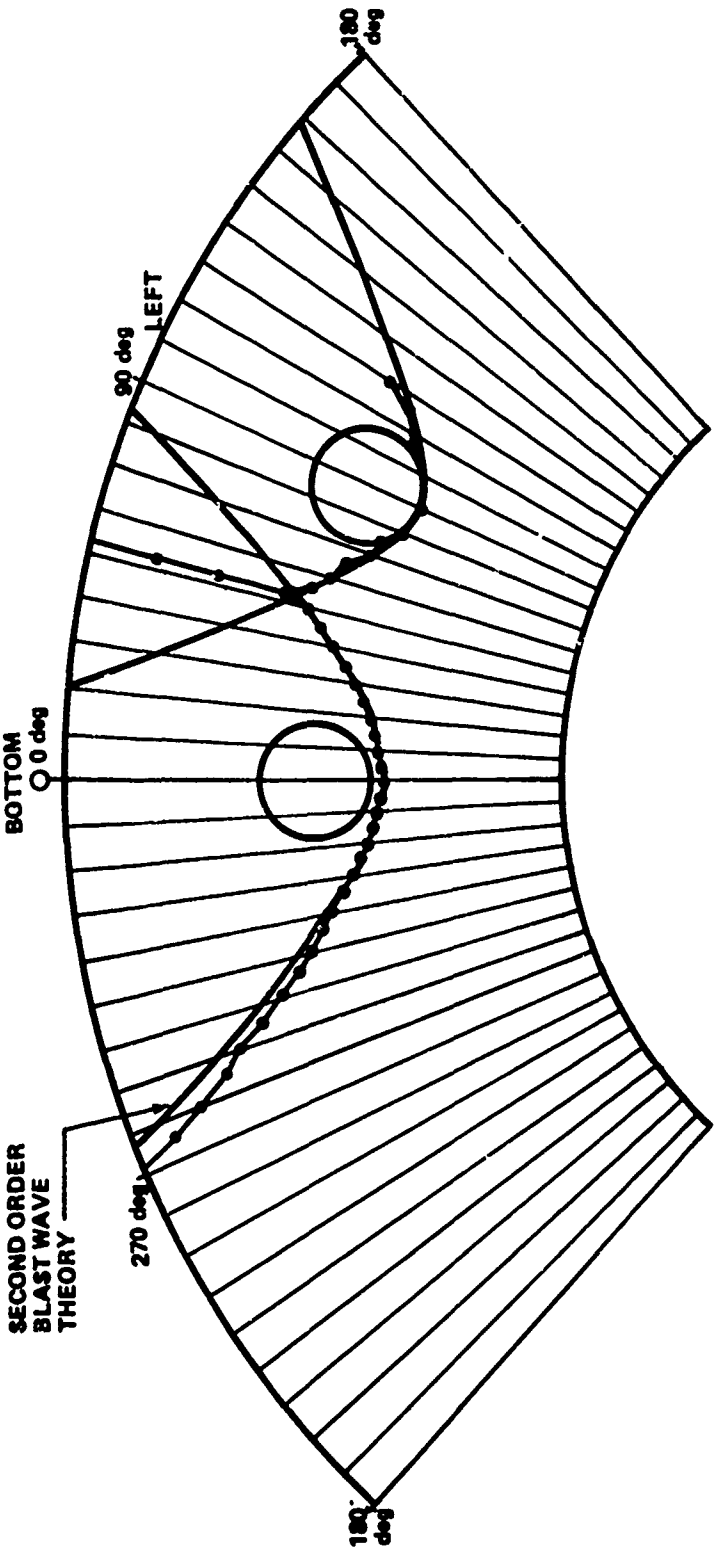


Figure 18. Shock Intersection, Run 14

## REFERENCES


1. Ferrari, C., Interference Between a Jet Issuing Laterally from a Body and the Enveloping Supersonic Stream, The John Hopkins University, Applied Physics Laboratory, April 1959, Bumblebee Report No. 286.

2. Amick, J. L. and Hays, P. B., Interaction Effects of Side Jets Issuing from Flat Plates and Cylinders Aligned with a Supersonic Stream, Wright Air Development Division, June 1960, Report No. TR 60-329.

3. Broadwell, James E., "Analysis of the Fluid Mechanics of Secondary Injection for Thrust Vector Control," AIAA Journal, 1, No. 5, May 1963, pp. 1067-1075. (See also Broadwell, James E., "Correlation of Rocket Nozzle Gas Injection Data," AIAA Journal, 1, No. 8, August 1963, pp. 1911-1913.)

4. Zukoski, Edward E. and Spaid, Frank W., "Secondary Injection of Gases into a Supersonic Flow," AIAA Journal, 2, No. 10, October 1964, pp. 1689-1696.

5. Charwat, A. F. and Allegre, J., "Interaction of a Supersonic Stream and a Transverse Supersonic Jet," AIAA Journal, 2, No. 11, November 1964, pp. 1965-1972.

6. Hsia, Henry T-S., "Equivalence of Secondary Injection to a Blunt Body in Supersonic Flow," AIAA Journal, 4, No. 10, November 1966, pp. 1832-1834.

7. Hsia, H. T-S., Seifert, H. S., and Karamcheti, K., "Shocks Induced by Secondary Fluid Injection," Journal Spacecraft, 2, No. 1, January-February 1965, pp. 67-72.

8. Wilson, W. G. and Comparin, R. A., "Analysis of the Flow-Disturbance and Side Force Due to Gaseous Secondary Injection into a Rocket Nozzle," Journal Spacecraft, 7, No. 5, May 1970, pp. 539-543.

9. Vickers, Inc., "Proportional Solid Propellant Secondary Injection Thrust Vector Control," November 1966, NASA CR-637.

10. Narasaki, T., "The Side Force Induced by an Obstacle in the Nozzle of a Rocket Engine," Paper presented to the XXI$^{st}$ International Astronautical Congress, Korstanz, Federal Republic of Germany, 4-10 October 1970.

11. Sakurai, A., "On the Propagation and Structure of a Blast Wave," Journal Phys. Soc. Japan, Part I: 8, No. 5, September-October 1953, pp. 662-669; Part II: 9, No. 2, March-April 1954, pp. 256-266.

12. Lees, L., "Hypersonic Flow," IAS Paper 554, 1955.

13. Ames Research Staff. Equations, Tables, and Charts for Compressible Flow, 1953, NACA 1135.

14. Ambrosio, A. and Wortman, A., "Stagnation Point Shock Detachment Distance for Flow Around Spheres and Cylinders," ARS Journal, 32, February 1962, p. 281.